Single fluorogen imaging reveals distinct environmental and structural features of biomolecular condensates

Authors: Tingting Wu[1,2], Matthew R. King[2,3], Mina Farag[2,3], Rohit V. Pappu[2,3*], Matthew D. Lew[1,2*]

Affiliations:

[1] Department of Electrical and Systems Engineering, Washington University in St. Louis, James F. McKelvey School of Engineering, Washington University in St. Louis; St. Louis, MO 63130, USA.

[2] Center for Biomolecular Condensates, James F. McKelvey School of Engineering, Washington University in St. Louis; St. Louis, MO 63130, USA.

[3] Department of Biomedical Engineering, Washington University in St. Louis, James F. McKelvey School of Engineering, Washington University in St. Louis; St. Louis, MO 63130, USA.

Corresponding authors. Email: pappu@wustl.edu; mdlew@wustl.edu

Abstract:

Recent computations suggest that biomolecular condensates that form via macromolecular phase separation are network fluids featuring spatially inhomogeneous organization of the underlying molecules. Computations also point to unique conformations of molecules at condensate interfaces. Here, we test these predictions using high-resolution structural characterizations of condensates formed by intrinsically disordered prion-like low complexity domains (PLCDs). We leveraged the localization and orientational preferences of freely diffusing fluorogens and the solvatochromic effect whereby specific fluorogens are turned on in response to the physico-chemical properties of condensate microenvironments to facilitate single-molecule tracking and super-resolution imaging. We deployed three different fluorogens to probe internal microenvironments and molecular organization of PLCD condensates. The spatiotemporal resolution and environmental sensitivity afforded by single-fluorogen imaging shows that the internal environments of condensates are more hydrophobic than coexisting dilute phases. Molecules within condensates are organized in a spatially inhomogeneous manner featuring slow-moving nanoscale molecular clusters or hubs that coexist with fast-moving molecules. Finally, molecules at interfaces of condensates are found to have distinct orientational preferences when compared to the interiors. Our findings, which affirm computational predictions, help provide a structural basis for condensate viscoelasticity and dispel the notion of protein condensates being isotropic liquids defined by uniform internal densities.

Main Text

Biomolecular condensates are thought to provide spatial and temporal control over cellular matter [1]. Proteins with intrinsically disordered regions (IDRs) such as prion-like low complexity domains (PLCDs) and arginine-glycine-rich (RG-rich) regions are prominent drivers of different types of condensates [2,3]. Recent investigations suggest that the simplest, single-component condensates formed by PLCDs and RG-rich IDRs, are viscoelastic fluids or solids [4-9]. The short-time behaviors of viscoelastic fluids are elastic whereas their long-time behaviors are viscous. Although it is expected that viscoelastic fluids should feature network-like internal structures [10,11], the spatial, nanoscale organization of molecules remains uncharacterized within simple one-component condensates, and more complex, multicomponent condensates.

Recent computational studies have predicted that within simple, one-component condensates formed by PLCDs, the protein molecules are organized to form spatially inhomogeneous networks [12,13] (**Fig. 1a**). Results from simulations suggest that internal networks in condensates have dynamic, hub-and-spoke organization with hubs being nanoscale clusters of molecules that are generated by reversible physical crosslinks among molecules [12,13]. These computational results challenge the prevailing view that condensates are isotropic liquids defined by uniform internal densities [14,15]. Here, we report results from experimental tests of computational predictions using state-of-the-art single-molecule tracking and single-molecule orientation localization microscopy (SMOLM). In these experiments, we combine freely diffusing fluorogenic probes [16-18] with single-molecule imaging [19-24] to characterize the internal solvent properties as well as the organization and dynamics of molecules within condensates. Our methods afford multiscale spatial and temporal resolution with single-molecule sensitivity to detect transient as well as persistent interactions. Our approach also enables characterizations of condensate microenvironments and time-averaged structures at distinct internal locations.

Fluorogenic molecules are environmentally sensitive probes. Their fluorescence intensities change in response to the dielectric properties and hydrophobicity of solvents (**Extended Data Fig. 1a, 1b**). Further, the emission spectra of solvatochromic dyes undergo pronounced shifts depending on their environments [16-18,25-27] (**Extended Data Fig. 1b**). We leveraged these effects to deploy fluorogenic molecules as structural probes in epifluorescence and super-resolution single-molecule imaging to investigate condensates formed by three sequence variants of the PLCD of hnRNP-A1 (A1-LCD) [2,28] and the RG-rich IDR from the protein DDX4 [3,29]. We focused on condensates formed by individual macromolecules, so-called single component condensates, to test the structural basis for measured viscoelastic properties [6,30,31] and predictions that have emerged from physical theory and computations [12,13,32].

In separate imaging measurements, we used different polarity-sensing fluorogens, namely, Nile blue (NB), Nile red (NR) [16,17], and merocyanine 540 (MC540)[18]. These fluorogens are dark in aqueous solutions, even when they are pumped with an excitation laser. As the fluorogens diffuse through solution, they can either partition into hydrophobic environments or bind specifically to hydrophobic pockets within or outside condensates. This binding causes an increase in their fluorescence quantum yield and a shift in their absorption and emission spectra, termed solvatochromism (**Fig. 1b**).

NR (**Fig. 1c, (i)**) is minimally soluble in aqueous buffers, and it has a solubility of 280 µM (0.09 mg/ml) in a 1:10 mixture of DMSO (dimethyl sulfoxide) and phosphate buffered saline (PBS). In contrast, NB (**Fig. 1c, (ii)**), which is essentially the same as NR, albeit with an amine,

has a solubility in water of 0.14 M (50 g/l). We used NR and NB as mutually cross-validating probes, whereby features discerned using both NB and NR can be taken to be robust to the structural aspects of the condensates as opposed to being consequences of the self-association of the dyes. MC540 (**Fig. 1c, (iii)**) partitions to interfaces between membranes and aqueous environments [18]. Accordingly, driven by the expectation that the interiors of condensates are likely to be microenvironments that are distinct from the coexisting phases [7,12,13,33,34] and thus delineated by interfaces, we used MC540 as a probe of condensate interfaces. Note that none of the proteins are chemically modified by dyes or other tags; instead, the fluorogenic dyes, which are present at micromolar concentrations in epifluorescence measurements and sub-micromolar concentrations in single molecule measurements, freely diffuse in solution and through the condensates [35]. Molecules that function as ligands can have a modulatory effect on the driving forces for phase separation. Ligands that stabilize dense phases, will lower the macromolecular saturation concentration (c_{sat}) whereas ligands that destabilize dense phases will have the opposite effect [36,37]. In contrast, passive clients will leave c_{sat} values unchanged. Before deploying the different fluorogens as probes, we measured their effect on the c_{sat} values of A1-LCD molecules. These measurements were performed at two different temperatures and different bulk concentrations of each of the dyes. The data show that effects of the dyes on the c_{sat} are negligible, being within the narrow errors of the measured c_{sat} values in the absence of the dyes (**Extended Data Fig. 2a-b**). Therefore, the dyes may be regarded as non-perturbing inert probes of the microenvironments of and internal organization within condensates.

We deployed the three different fluorogens (NR, NB, and MC540) in epifluorescence as well as single-molecule measurements. In the latter, we measure digital on / off blinking of the fluorogens within "hotspots" that are formed by the macromolecular scaffolds of condensates. The hotspots are not aggregates of dye molecules. Instead, they are single fluorogens turning on and off via binding and unbinding / photobleaching. Additionally, the microscope we use is sensitive to single molecules. If the internal concentrations of dyes were anywhere near their saturation concentrations, then the background fluorescence would swamp the fluorescence of individual molecules. As summarized below, we do not have any such challenges in our single-molecule measurements. Further, given our findings of increased fluorescence intensity within the dense phase, which we interpret to mean that the dense phase is more hydrophobic than the dilute phase, each fluorogen will be brighter within condensates and aggregation of dyes should be very easy to detect. Instead, we observe that the fluorescence from diffusing fluorogens is extremely weak in regions within the hydrophobic dense phase that are localized away from the hotspots. This would not be true if the dyes undergo aggregation within the condensates. Importantly, we also cross-validate our findings regarding internal structures of condensates using NB and NR as probes. NB is considerably more soluble than NR, and in the single molecule measurements, we used NB at concentrations that are three orders of magnitude lower than that of NR. We present the results from both sets of dyes, and the findings regarding internal structures within condensates are consistent across both dyes.

Interiors of A1-LCD condensates are more hydrophobic than coexisting dilute phases.

In bulk epifluorescence imaging, each of the three fluorogens exhibits stronger fluorescence signal from within condensates than from the coexisting dilute solutions. However, each of the fluorogens perceive and sense the environments of condensates differently because of the different environmental sensitivities of the fluorogens (**Fig. 1c-e**). The fluorescence intensity of NB is considerably more uniform throughout each condensate. This uniformity is indicative of

a more homogenous distribution of binding sites for NB (**Fig. 1c**). In contrast, NR fluorescence is clustered into hubs that are twice as bright as their background (**Fig. 1d**). Hubs are observable in condensates that form on and above the coverslip (**See Movie S1**). These data suggest that NR fluoresces in response to specific environmental properties and molecular architectures within condensates. The overall higher fluorescence intensities of NR and NB within condensates indicate that the internal environments of condensates are more hydrophobic than coexisting dilute phases. This interpretation is bolstered by the fact that the fluorogens are essentially dark in the dilute phase.

MC540 is a bipolar molecule, and this property enables it to fluoresce strongly at the interface between distinct environments [38]. In accord with this expectation, we find that MC540 is brightest at condensate interfaces (**Fig. 1e**). Condensates deform as they adsorb onto coverslips, and fluorogens track the internal rearrangements as they happen (**Extended Data Fig. 3**): NB fluorescence is uniform across each condensate; clusters of NR molecules move apart from one another; and the strong MC540 fluorescence at the condensate interface dissolves into a more uniform distribution as the condensates adsorb to and wet the coverslip (**Fig 1e** and **Fig. S2a, S2b)**. In summary, NR, NB, and MC540, three chemically distinct, freely diffusing fluorogens, each reveal distinct structures within and surrounding single-component A1-LCD condensates. Although MC540 has negligible impact on bulk phase separation (**Extended Data Fig. 2**), our epifluorescence images revealed that MC540 can alter condensates when they adsorb onto coverslips (**Fig. S2c**). This effect is eliminated by lowering the concentration of MC540. Accordingly, to avoid perturbing influences of MC540 on condensates, we used sub-micromolar concentrations (0.25 μM) of MC540 and image unwetted condensates for all our measurements.

Fluorogens uncover inhomogeneous spatial organization of proteins within condensates.

The epifluorescence data are suggestive of internal inhomogeneities that are sensed differently by each of the three different dyes. To compare how the different fluorogens perceive internal structures, we imaged single condensates sequentially using NB and NR. Both NB and NR localize to hubs in similar spatial locales. The presence of hubs is made clear by the fact that localized signals from freely diffusing fluorophores rise above a uniform background fluorescence within condensates (**Fig. 1f, 1g**). However, the hubs always appear with much better contrast above background when using NR compared to those accessible to NB (**Fig. 1g** inset). Further, we observed additional hubs with NR when compared to NB.

The excitation and emission spectra of NR shift towards blue wavelengths in solvents that are non-polar when compared to water (**Extended Data Figure 1f**) [39]. To ascertain if environments are spatially inhomogeneous within condensates, we imaged the dyes in two separate wavelength regimes using orange (593 ± 23 nm) and red (676 ± 18 nm) bandpass filters (**Fig. 1h, 1i**). We detected mostly uniform NR fluorescence within the red emission window. However, in the orange emission window, the background fluorescence nearly disappears while the hubs for NR persist. These data suggest that the hubs where NR localizes are more hydrophobic than the interiors of condensates, which in turn are more hydrophobic than the coexisting dilute phases.

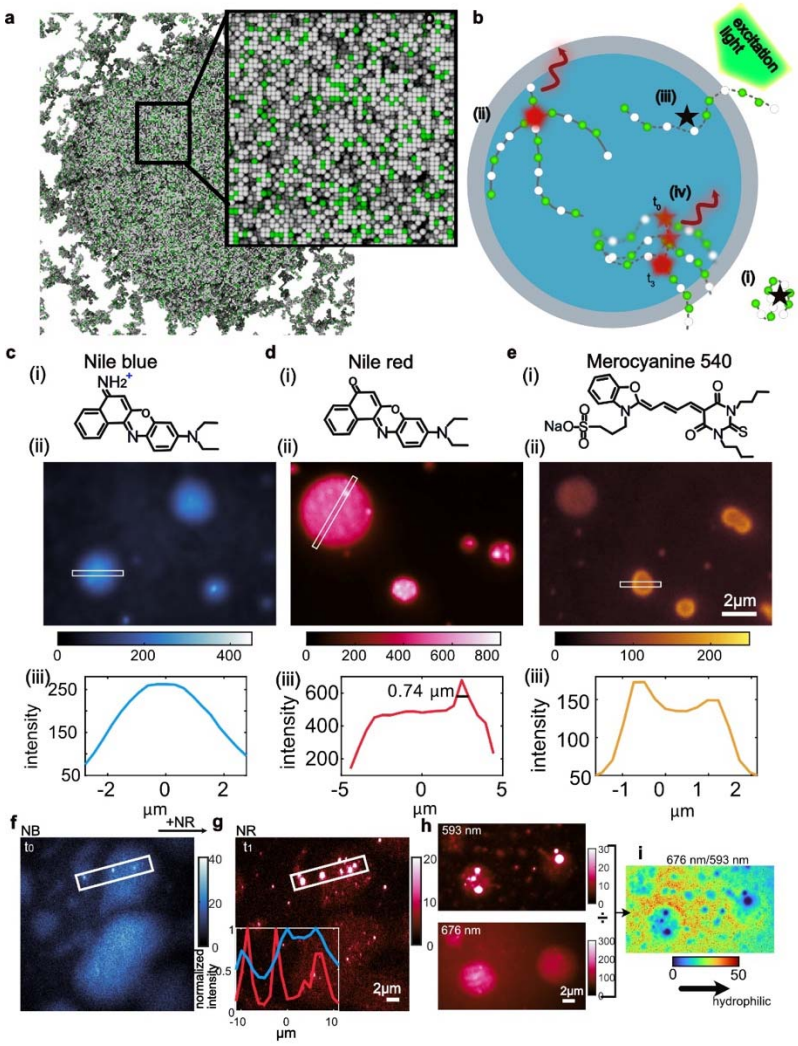

Fig. 1. Fluorogenic probes sense the distinct chemical environments inside biomolecular condensates. a: The motivation for our experiments comes from lattice-based simulations of phase separation and the structures of condensates formed by PLCDs [12,13]. Here, we show a snapshot depicting the network-like internal organization of A1-LCD molecules within condensates generated using LaSSI simulations. Green and white beads are the aromatic stickers and non-aromatic spacers, respectively. Grey beads are solvent-filled voids [12]. **b**: As fluorogens (shown as stars) diffuse through solution, they encounter different chemical environments in the dilute phase (white space), in the condensate (large blue circle), and in the interface between the dilute phase and condensate (gray space). In response, they either (i, iii) remain dark (black stars) or (ii, iv) emit fluorescence (red stars and arrows). Their (ii, iv) speeds and brightness are also affected. **c-e**: Imaging A1-LCD condensates using (c) Nile blue (NB), (d) Nile red (NR), and (e) merocyanine 540 (MC540). (i) Chemical structures of the three different fluorogens. (ii) A1-LCD condensates as imaged by epifluorescence microscopy. (iii) Fluorescence intensity profiles along the long axis of white box shown in (ii). **f**, **g**: Epifluorescence images of condensates collected using (f) NB, and then adding (g) NR. Inset: Fluorescence intensity profiles (blue: NB, red: NR) along the long axis of the white boxes shown in (**f, g**). **h**: NR epifluorescence microscopy of A1-LCD condensates collected using two emission windows (top: 593 ± 23 nm and bottom: 676 ± 18 nm). Fluorescence collected in the orange emission window (593 nm) was excited using a 532-nm laser, and fluorescence collected in the red emission window (676 nm) was excited using a 637-nm laser. **i**: The intensity ratio between images captured in red and orange emission windows, respectively. Color bars: c-h, photon counts; i, intensity ratio.

Single-molecule imaging shows that spatial inhomogeneities extend down to the nanoscale.

We leveraged the diffusion and transient binding of NB and NR [35,40] as a photo-switching ("blinking") mechanism for super-resolution, single-molecule localization microscopy (SMLM) [41-44]. As individual probes diffuse through solution, they remain dark until they find themselves in hydrophobic environments or bind to hydrophobic sites. When they encounter hydrophobic pockets, they become bright, and the fluorogens become dark again when they leave these pockets [19]. Accumulating the positions of many blinking events yields detailed SMLM maps of internal structures within condensates with nanoscale resolution and single-molecule sensitivity (**Movie S2**).

Super-resolution images of single condensates show that both NR and NB exhibit non-uniform localization patterns that persist for several minutes (**Fig. 2a, 2b**). Again, we observed hubs, this time at the nanoscale, in images collected using both NR and NB (**Fig. 2c**). To quantify the spatial inhomogeneity using single-molecule blinking (**Fig. 2d**), we calculated the excess variance within each condensate. If a fluorogenic probe has a uniform probability of blinking across the entire condensate, its localization density would be Poisson-distributed [45]; this behavior would yield an excess variance of zero (**Fig. S3**). The condensates imaged sequentially by NB and NR showed larger than expected variances with a mean variance of 1.3 ± 0.8 (std. dev., 2.1×10^4 localizations/condensate on average). Thus, SMLM shows that both NB and NR exhibit large and significant spatial variations in their blinking dynamics (**Fig. 2d**).

The super-resolution images of NR show the presence of inhomogeneities or hubs at spatial scales that lie below the diffraction limit (**Fig. 2c**). Next, we measured the relative proportion of localizations that are spatially clustered to quantify the relative affinities of NR and NB for binding to nanoscale hubs (**Fig. 2e, 2f)**. For each localization, we compared the local density to the surrounding density and computed a clustering coefficient [46,47]; molecules with clustering coefficients above a threshold of 20 are classified as being clustered (**Fig. 2e**, see Methods). For the five condensates imaged by NR and NB, 27% ± 3% of NR molecules and 13% ± 4% of NB molecules were clustered. This indicates that clustering is detected twice as often with NR when compared to NB. The implication is that the NR binds more strongly to nanoscale clusters within condensates than NB.

For mapping hubs with single-molecule sensitivity and nanoscale resolution, it is necessary that fluorogen binding events persist for at least ~10 ms, thus matching the exposure time of the camera. We quantified the similarities and differences between spatial inhomogeneities mapped by NR and NB [48,49]. For images collected using both NR and NB, we found that the diffuse regions, as sensed by the extent of binding to a region, are mostly uncorrelated. However, regions where NR and NB localize preferentially are highly correlated with one another (**Extended Data Fig. 4**).

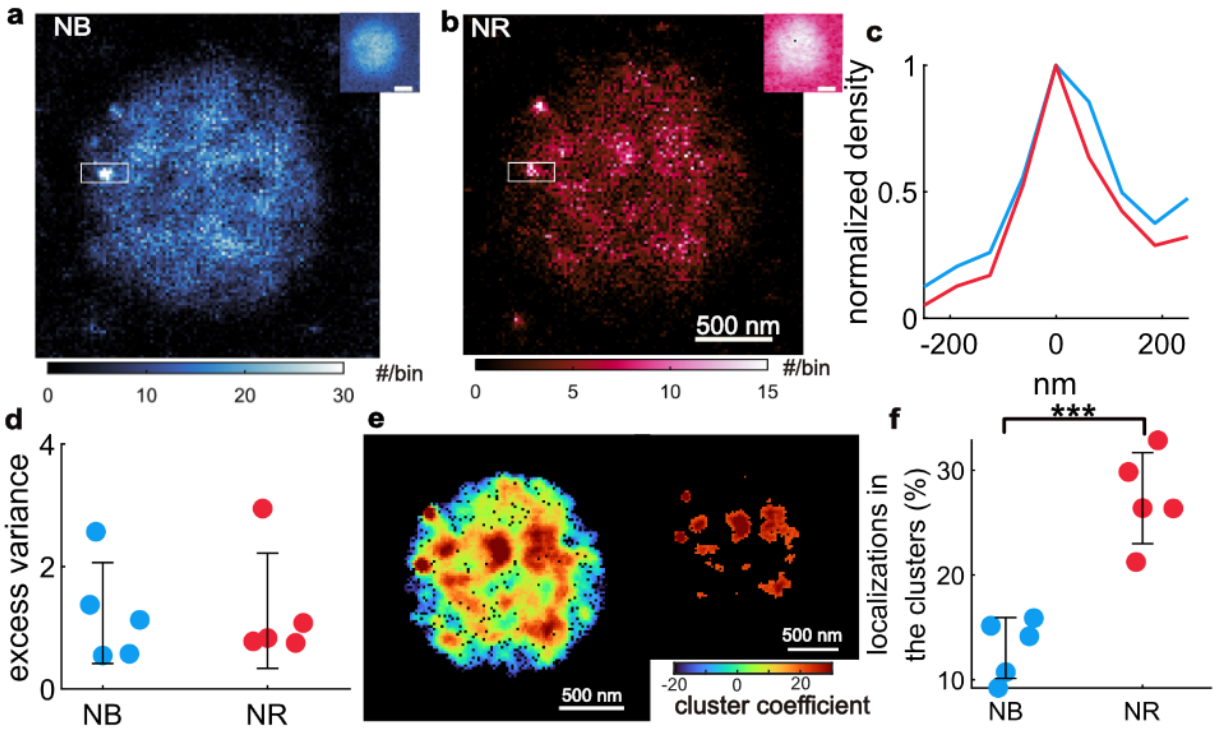

Fig. 2. Single molecule localization microscopy (SMLM) of NB and NR reveals that they bind to molecules that are organized into nanoscale clusters within condensates. a, **b**: SMLM images of a single A1-LCD condensate collected using (**a**) NB and (**b**) NR. Top insets: epifluorescence images. Color bars: number (#) of single-molecule localizations within each 20 nm × 20 nm bin. **c**: Localization profile along the long axis of the white box shown in (**a, b**). **d**: Quantifying the binding and activation of NB (blue) and NR (red) within five condensates using excess variance. Larger excess variance values represent greater heterogeneities in the blinking statistics of fluorogenic probes within a condensate; zero excess variance represents uniform blinking statistics throughout the condensate. **e**: A1-LCD condensate in (**b**) imaged by NR and color-coded by clustering coefficient; molecules with clustering coefficients above a threshold of 20 are classified as being clustered. Inset: map of regions that contain clustered NR localizations. **f**: Percentages of single-molecule localizations that are spatially clustered for five condensates.

Single-molecule tracking shows slow moving nanoscale hubs that coexist with fast moving molecules.

Our data indicate that the nanoscale hubs represent clusters of protein molecules that contribute preferred local environments and high avidity of binding sites for the different fluorogens. Single-molecule imaging also shows that nanoscale hubs within each of the condensates disappear from one location and reappear at nearby locations (**Movies S3 and S4**). We probed these dynamics inside condensates by tracking the movements and fluorescence burst durations of individual fluorogens (**Movie S5**). The burst duration t_b is correlated with the amount of time a fluorogen spends in a fluorescence-promoting environment. The speed measures the distance covered by a fluorescing probe at 10 ms intervals (**Fig. 3a**, **Extended Data Fig. 5**). As a fluorogen explores a condensate, changes in the local environment cause both its burst duration and speed of movement to vary. For example, the burst durations of NR range from 10 ms to more than 170 ms (**Fig. 3b**). This heterogeneity is highlighted by reconstructing SMLM images using only single molecules with short burst durations ($t_b \leq 60$ ms, **Fig. 3c**) versus those with long burst durations ($t_b > 60$ ms, **Fig. 3d**). Single molecules with short burst

durations are distributed uniformly across the condensate, while hot spots are dominant in the long-burst duration images. This trend was also observed when the condensates were imaged using NB, thus providing mutual cross-validation of the results regarding hub dynamics (**Extended Data Fig. 5i-5k**). However, when compared to NR, NB exhibits larger displacements (**Extended Data Fig. 5b,5d**).

We separated NB emitters into three categories based on their speeds that were measured between consecutive frames (10 ms exposure times, **Fig. 3e**). An SMLM image, reconstructed from high-speed emitters, shows a uniformly distributed localization density across the condensate (**Fig. 3f**), while an SMLM image reconstructed solely from low-speed emitters exhibits clusters and nonuniform localization patterns (**Fig. 3g**). This phenomenon is consistent across six different A1-LCD condensates where the average excess variance of single-molecule images reconstructed using emitters with low, medium, and high speeds of emitters are 0.84 ± 0.33, 0.13 ± 0.06, and 0.05 ± 0.04, respectively (**Fig. 3h**). Condensates imaged using NR showed similar trends (**Extended Data Fig. 5e-5g**). Overall, NR and NB emitters with longer burst durations tend to have lower speeds (**Fig. 3i**). The hubs revealed by longer-burst emitters and those sensed by slowly moving emitters are consistent with one another (**Fig. 3** and **Extended Data Fig. 5**).

To provide a physical interpretation for why NR and NB dyes are trapped for longer periods of time at hubs, we analyzed published results from lattice-based LaSSI simulations [12]. PLCDs are biological instantiations of linear associative polymers featuring cohesive motifs known as stickers that are interspersed by solubility-determining spacers [50]. In the simulations, the interactions for A1-LCD and related PLCDs follow a hierarchy whereby interactions between aromatic residues are the strongest [12]. Stickers form reversible physical crosslinks with one another, whereas spacers modulate sticker-sticker interactions and the coupling between phase separation and percolation [50]. Aromatic residues of A1-LCD and related PLCDs function as stickers that enable physical crosslinking of these molecules [2,28]. Conversely, charged, and polar residues interspersed between the stickers act as spacers [2,28]. The simulations of Farag et al.[12] showed that the spatial inhomogeneity and network connectivity within PLCD condensates are governed by the valence of stickers [28] and the differences in interaction strengths between different stickers and spacers [12].

We reasoned that the nanoscale hubs uncovered using NR and NB are direct readouts of networked A1-LCD molecules formed via reversible, intermolecular physical crosslinks among aromatic stickers. Accordingly, we probed the correlation between molecular displacements and the extent of crosslinking in the simulated condensates. These simulations show that A1-LCD molecules that are part of densely crosslinked networks have smaller overall displacements (**Fig. 3j**). The simulations suggest that nanoscale hubs observed using single fluorogen imaging are clusters of A1-LCD molecules defined by the density or extent of physical crosslinking. The fluorogens become trapped for longer times in nanoscale hubs because of the higher local density of stickers within the clusters that underlie the hubs.

Physical crosslinks are likely to be the source of time-dependent elastic moduli of A1-LCD condensates that have been measured recently by Alshareedah et al., [31]. The presence of physical crosslinks, which translates into nanoscale hubs, will build up local shear stress. Movement of the hubs is a form of shear strain that releases the stress. The timescales for shear stress relaxation have been estimated by Ghosh et al.[5] to be on the millisecond to seconds timescales, and this is consistent with the timescales we have measured for the movement of

nanoscale hubs. Therefore, we interpret the movement dynamics of hubs to be indicative of shear stress relaxation dynamics in the networks formed by A1-LCD molecules.

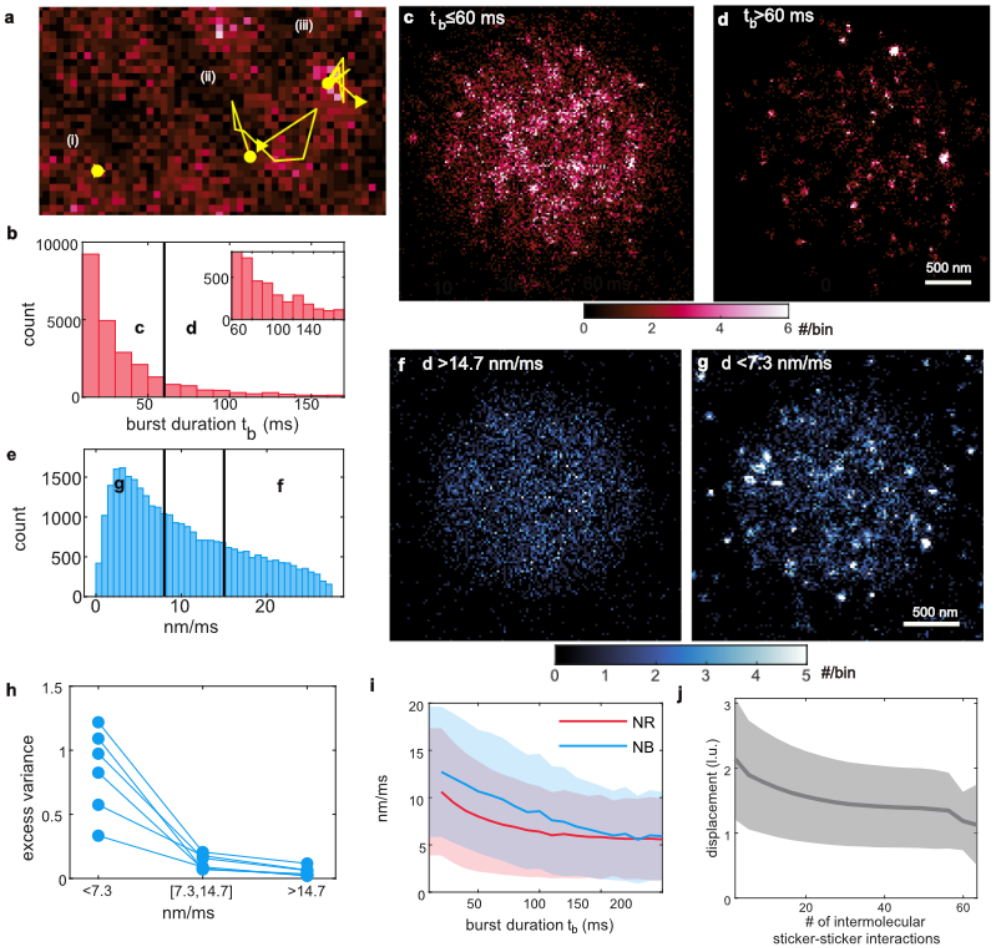

Fig. 3. Tracking of single-molecule fluorescence burst durations and speeds uncover inhomogeneous molecular organization and dynamics within condensates. a: Single NR fluorophores exhibit both (**i**) short and (**ii, iii**) long burst durations, as well as (**ii**) high and (**iii**) low speeds. **b:** burst duration t_b of NR. **c, d:** SMLM images of NR molecules with burst durations (**c**) shorter than 60 ms and (**d**) longer than 60 ms. **Extended data Fig. 5 j-k** shows burst duration data for NB. **e:** Speed distribution of NB measured between consecutive camera frames (10 ms exposure time). **f, g:** SMLM images of NB molecules with speeds (**f**) larger than 14.7 nm/ms and (**g**) smaller than 7.3 nm/ms. **Extended data Fig. 5 e-g** shows speed data for NR. **h:** Excess variance of NB localizations grouped by speeds (left: <7.3 nm/ms, middle: between 7.3/ms and 14.7 nm/ms, right: >14.7 nm/ms). Blue lines: excess variance of NB within each condensate. **i:** Speeds of NB (blue) and NR (red) as a function of their fluorescence burst durations. Lines: mean value averaged over 150,000 trajectories for NB and 129,000 trajectories for NR; shaded region: ±1 standard deviation. **j:** Displacement in lattice units (l.u.) of each chain within a simulated A1-LCD condensate as a function of the number of intermolecular sticker-sticker interactions. Results are from lattice-based Monte Carlo simulations [12].

Valence of aromatic residues impacts nanoscale dynamics of PLCDs within condensates.

Martin et al., and Bremer et al., showed that the driving forces for phase separation of A1-LCD and designed variants thereof are governed by the valence, i.e., number, and types of aromatic residues [2,28]. We used NR and NB dyes to obtain comparative assessments of nanoscale structures within condensates formed by two variants of the A1-LCD system designed by Martin et al. and designated as Aro^+ and Aro^-. The Aro^+ variant has more aromatic residues dispersed

uniformly along the linear sequence when compared to the wildtype A1-LCD while the Aro$^-$ has fewer aromatic groups [28] (**Fig. 4a, Table S1**).

When probed using NB, the condensates formed by Aro$^+$ demonstrated the longest burst duration with an average of 43 ms. In contrast, when probed using NB, the condensates formed by Aro$^-$ show an average duration of 26 ms (**Fig. 4b**). Note that while dense phase concentrations of proteins change minimally within the condensates formed by different variants [2,12,28], the LaSSI simulations suggest that the extents of crosslinking vary with the valence of aromatic residues [12]. We revisited the simulation results and obtained quantitative comparisons, which show that the numbers of sticker-sticker interactions, quantified within simulated condensates, are highest in those formed by Aro$^+$ and lowest in those formed by Aro$^-$ (**Fig. 4c**). Based on these comparisons, we infer that the longer burst durations for NB in Aro$^+$ condensates are attributable to the higher valence of aromatic residues, which results in higher extents of physical crosslinking, and longer-lasting nanoscale hubs that trap NB for longer times and lead to longer fluorescence bursts. In contrast, condensates formed by Aro$^-$ feature fewer sticker-sticker interactions, and this leads to lower affinities and shorter burst durations when the condensates are probed using NB. Similar data were obtained when the condensates were probed using NR (**Extended Data Fig. 6**).

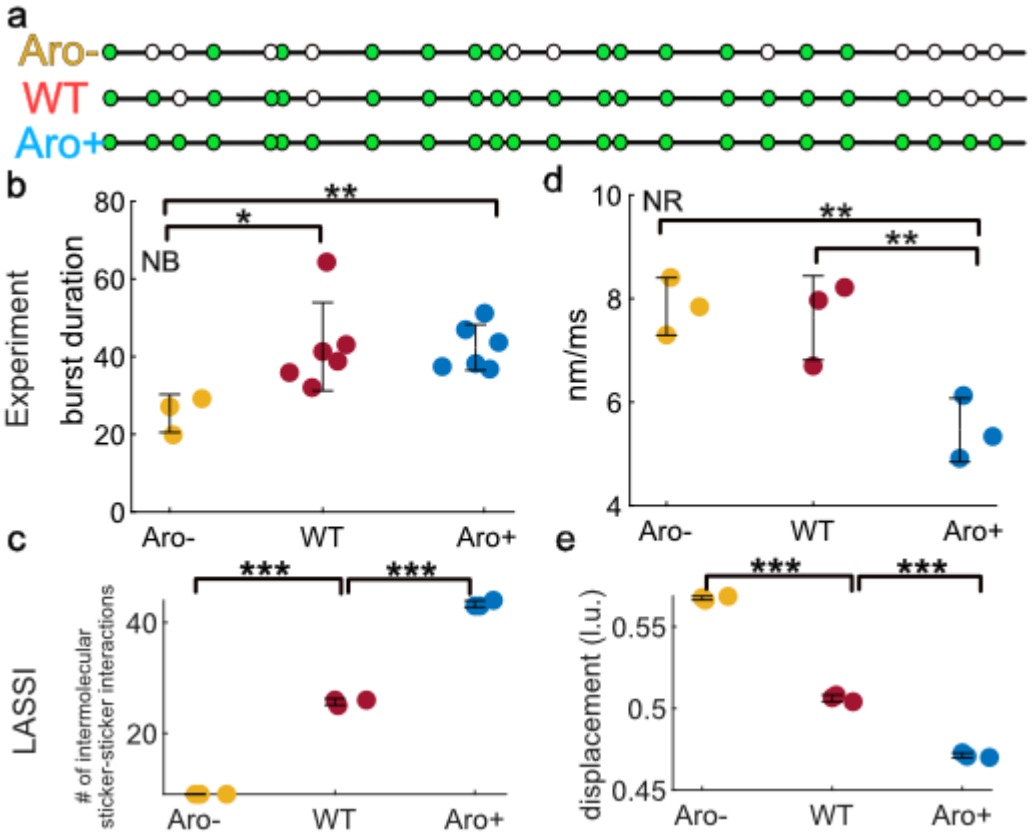

Fig. 4. Nanoscale dynamics within condensates are influenced by the numbers of aromatic residues. a: Schematic showing the positions of aromatic amino acids as green circles in Aro$^-$, A1-LCD (WT), and Aro$^+$ variants. **b**: Fluorescence burst durations for the three condensates measured using NB. **c**: Number of intermolecular sticker-sticker interactions in simulated condensates. The sequence-specific simulations were performed using the LaSSI

engine. **d**: Speed of NR within condensates formed by Aro^{-}, WT, and Aro^{+}. **e**: Displacements of protein chains quantified in simulated condensates. Circles in (b) represent the average burst durations of individual condensates, and in (d-e) they represent the median values of measurement parameters for individual condensates. Error bar: mean ± one standard deviation.

Molecular transport within condensates will be governed by at least two types of dynamics *viz.*, the lifetimes of physical crosslinks and the timescales for displacements of molecules. These dynamics can be probed by measuring the speeds of fluorogen displacements. The speeds serve as useful proxies for evaluating how crosslinks, which generate locally elastic networks, impede the mobilities of fluorogens, thereby probing the local viscosity within condensates. Our single-molecule tracking measurements indicate that NR moves fastest in Aro^{-} condensates with an average speed of 8.9 nm/ms. In contrast, NR moves most slowly in Aro^{+} condensates with an average speed of 6.7 nm/ms (**Fig. 4d**). These observations indicate that the extent of crosslinking engenders restrictions to the movements of fluorogens. These observations are in line with findings from LaSSI simulations, which show that proteins in Aro^{+} condensates have the smallest displacements, whereas proteins in Aro^{-} condensates have the largest displacements of the three simulated condensates (**Fig. 4e** and **Extended Data Fig. 7**).

Single-molecule orientation localization microscopy reveals distinct features of interfaces.

Computations predict that A1-LCD molecules have a clear preference for non-random orientations at interfaces of condensates [12]. For PLCDs at the interface versus interiors of condensates, Farag et al.[12] computed the projections of end-to-end vectors within A1-LCD molecules onto radial vectors that connect sites on chains to the center of a condensate. They observed that individual molecules are randomly oriented within condensates, and there is a statistically significant bias toward perpendicular orientations with respect to the interface. In follow-up work, Farag et al.[13] showed that the orientational preferences are more pronounced for PLCDs that are stronger drivers of condensation, because perpendicular orientations help minimize the number of unsatisfied stickers at the interface.

In epifluorescence imaging, we observed strong fluorescence signals from MC540 at the interface of the condensates (**Fig. 1e**). The fluorescence of MC540 is influenced by the equilibrium between dimer and monomer states of MC540, where monomers are fluorescent and dimers are non-fluorescent [38]. This dimer-monomer equilibrium is strongly influenced by the molecular organization of the local environment [51].

Given the strong fluorescence signals we observed for MC540 at the interface, we leveraged polarized epifluorescence microscopy to probe the orientational preferences sensed by this fluorogen. We separate the fluorescence emission from MC540 into x- and y-polarized channels (I_x, I_y). We then calculate the linear dichroism (LD) as the ratio: $(I_x - I_y)/(I_x + I_y)$, which takes values from –1 to +1. An LD near +1 signifies that the x-polarization dominates the fluorescence emission, whereas a negative LD near –1 indicates dominance of the y-polarization. We noticed that transitioning from Aro^{-} to Aro^{+}, the condensates exhibit increasingly discernible pink and green hues at the interfaces of condensates, indicating a stronger polarization preference at the interface (**Fig. 5a**). For Aro^{+}, we observed mostly x-polarized fluorescence at the top and bottom edges and y-polarized fluorescence at the left and right sides (**Fig. 5a**). Comparing Aro^{+}

with Aro^- and WT, we note that the LD distribution for Aro^+ is broader and encompasses more instances with large absolute LD values (**Fig. 5b**).

To obtain deeper insights regarding the orientational preferences recorded by epifluorescence imaging, we turned to single-molecule imaging. While the SMLM images show a high density of MC540 at the interface of LCD condensates (**Fig. 5c**), they do not provide insights into how MC540 binds to the proteins. Thus, we went beyond SMLM and to employ single-molecule orientation localization microscopy (SMOLM) for measuring both the 3D position and orientation of MC540 (**Extended Data Fig. 8 and Movie S6**). SMOLM uses a pixOL phase mask to encode the information of 3D position and orientation into the intensity distribution of SM blinking events [52]. We quantified orientational preferences by quantifying the angle, denoted as δ, which is the measured angle of MC540 in relation to the normal vector to the condensate interface (**Fig. 5d**). The SMOLM images, color-coded according to δ and referred to as δ-SMOLM, indicate that freely diffusing MC540 dyes have a statistically significant preference for orientations parallel to the condensate interface (depicted in bluish hues in **Fig. 5d**). This orientational preference is observed at the interfaces of all three PLCD condensates (**Fig. 5d**). When comparing the median δ values across multiple condensates for the three LCD variants, we observed that Aro^+ exhibits the highest δ value, with a mean of 61˚, while Aro^- and WT have similar mean values of δ, which are 57˚ and 56˚, respectively (**Fig. 5e**).

The PLCD molecules drive condensate formation, and in accord with established nomenclature, we refer to them as scaffolds [1]. At the concentrations used in our experiments, the fluorogenic dyes interact minimally with one another. Instead, they localize and bind to sites on the scaffold molecules. Fluorogens such as MC540 localize preferentially to the interface and engage in heterotypic interactions with scaffolds. The fluorogens do not influence the driving forces for phase separation because their interactions are weaker than the homotypic inter-scaffold interactions. Accordingly, and in line with recent work, MC540 may be viewed as an adsorbent, whereas the PLCD molecules are the scaffolds [53]. Erkamp et al., recently showed that whereas scaffolds show statistical preference for perpendicular orientations, adsorbents show a statistical preference for parallel orientations to the normal vector at condensate interfaces [53]. Our SMOLM data for MC540 are in line with this expectation. Unlike the adsorbents, scaffolds should have a statistical preference for perpendicular orientations. This expectation was confirmed using results from LaSSI simulations, which show that scaffold molecules have a statistical preference for perpendicular orientations, i.e., smaller δ values **(Fig. 5f** and **Extended Data Fig. 9**). The observed orientational preferences become more pronounced as the interactions among scaffolds become stronger with increasing numbers of aromatic residues **(Fig. 5f)**. Taken together with the simulation results, the SMOLM data, obtained using MC540, highlight the unique interfacial features of condensates.

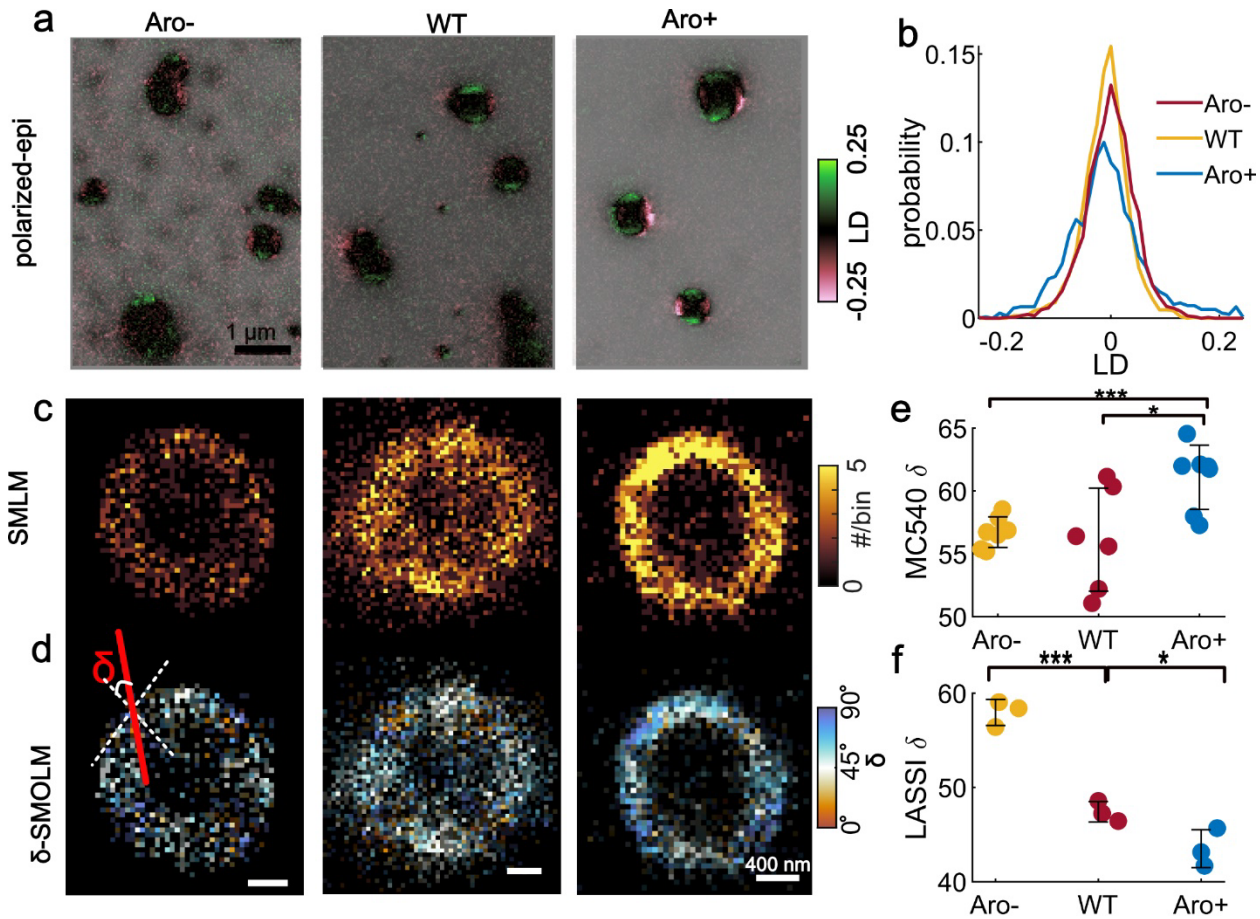

Fig. 5. MC540 preferentially localizes to interfaces and displays distinct orientational preferences. a: Linear dichroism (LD) of MC540 measured by polarized epifluorescence imaging. **b:** LD distributions quantified from images shown in (**a**). **c:** SMLM images of MC540. **d:** Orientation angles δ for MC540 measured with respect to the normal vector to the condensate interface using SMOLM; the median angle δ is depicted within each 50 nm × 50 nm bin. **e:** Median δ values computed across individual condensates (circles). Error bar: mean±1 standard deviation. **f:** δ values computed from LaSSI simulations using orientations of protein molecules at the interface.

Discussion

In this work, we used freely diffusing, environmentally sensitive fluorogens in epifluorescence imaging and super-resolution SMLM as well as SMOLM to probe the internal and interfacial structures of condensates formed by PLCDs. Fluorogen-based imaging of condensates is a unique, non-perturbative approach that does not require labeling of scaffolds or other condensate components using fluorescent proteins or dyes [54]. Accordingly, fluorogen-based imaging in all three modes, especially SMLM and SMOLM, offers multiscale spatial and temporal resolution information with single-molecule sensitivity. The methods are especially powerful when multiple fluorogens are deployed independently because the different dyes sense and see the same condensates differently.

Overall, the picture that emerges from single fluorogen imaging is concordant with recent computational studies and may be summarized as follows (**Fig. 6**): The interiors of condensates are more hydrophobic than the coexisting dilute phases. This picture is also in line with recent

inferences based on partitioning studies of small molecules that include drugs and drug-like molecules [55]. Within condensates, we observe nanoscale spatial inhomogeneities. That the inhomogeneities represent distinct local environments is made clear by the observation that the signals obtained using NB are more uniform than the signals obtained using NR. These fluorogens are differently sensitive to hydrophobic environments, with NR having a higher sensitivity. Inhomogeneities are manifest as nanoscale hubs because the fluorogens, particularly NR, bind preferentially to hubs that are more hydrophobic than the background of the condensate. The nanoscale hubs have a greater ability to trap fluorogens thus providing stable binding sites for them to blink for longer times. Finally, SMOLM imaging suggests that the interface between dilute and dense phases is a unique environment where MC540 molecules show marked orientational preferences. Increasing the number of aromatic stickers increases the ability to trap dyes in the interior and impact the orientational preferences of dyes at the interface.

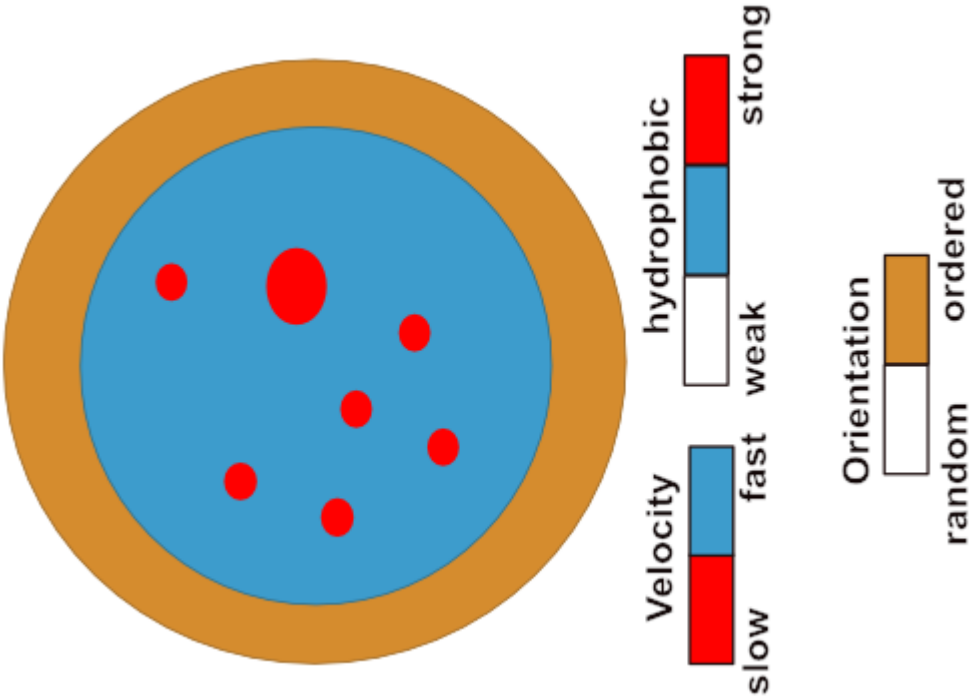

Fig. 6. Schematic summarizing the structural features of condensates that were inferred from the fluorogenic experiments. Condensates are more hydrophobic than their coexisting dilute phases. They feature spatial inhomogeneities that are manifest as nanoscale hubs (red regions). Hubs are more hydrophobic compared to other regions (blue) within condensates, as well as to the dilute phase (white area). Fluorogens bound to nanoscale hubs move more slowly compared to other regions. Proteins at the interface (orange) have distinct orientational preferences that are unmasked by specific fluorogens such as MC540.

Other archetypes of low complexity domains that are drivers of condensate formation include RG-rich IDRs such as the N-terminal domain from the RNA helicase DDX4 [3,29] (**Extended Data Fig. 10**). As with A1-LCD, we found that NB shows relatively uniform fluorescence, which is suggestive of a more hydrophobic interior when compared to the coexisting dilute phase. NR is concentrated into hubs, and MC540 again preferentially localizes to the interface, highlighting the unique environment of the interface when compared to the interiors of condensates. Although the molecular grammars of RG-rich IDRs are different from those of PLCDs [12], these domains appear to form condensates that respond in similar ways to NB

and NR. This similarity is not surprising given recent findings regarding the π-character of arginine residues [56], and their apparent hydrophobicity [57] as probed by how water molecules organize around arginine sidechains [58]. However, and in contrast to condensates formed by PLCDs and the RG-rich IDR of DDX4, the condensates formed by polynucleotides such as poly-rA respond very differently to NR (**Extended Data Fig. 10**). If there are spatial inhomogeneities and multiscale hubs within RNA condensates, they are not sensed by NR. The implication is that different types of fluorogens, specifically intercalating dyes, will be needed to probe the internal organization of RNA-rich condensates.

The existence of inhomogeneities, albeit on the micron-scale, has been well established for multicomponent systems such as stress granules [59], nucleoli [60], nuclear speckles [61], the mitochondrial nucleoid [34], and synthetic systems comprising two or more macromolecular components [62,63]. Our work highlights the existence of spatial inhomogeneities on the nanoscale for the simplest of systems namely, condensates formed by one type of macromolecule in a solvent. We have shown how the titration of stickers affects the observed inhomogeneities. We also show that the presence of inhomogeneities is not unique to condensates formed by PLCDs. Overall, our observations provide a structural rationale for reports that condensates formed by low complexity domains are viscoelastic materials [4,7,8] with dynamical moduli that have sequence- or architecture-specific relaxation times [6]. The spatial inhomogeneities give condensates a sponge-like appearance. This rationale is intriguing partly because it is consistent with inferences made by Handwerger et al., who conjectured, based on quantitative analysis of differential interference microscopy images, that membraneless nuclear bodies including nucleoli, nuclear speckles, and Cajal bodies have sponge-like structures [64]. Our findings, taken together with the postulates of Handwerger et al., suggest that multicomponent condensates that are characterized by micron-scale inhomogeneities might also feature nanoscale inhomogeneities that we have characterized here. Generalizing our methods to characterize multicomponent systems is currently underway. To probe region-specific inhomogeneities, this effort will require functionalizing the fluorogens with peptide-based probes of molecular grammars that define distinct regions within larger, inhomogeneously organized multicomponent condensates.

Overall, our work represents the first multiresolution attempt at direct experimental observation of inhomogeneities within condensates that leads to their descriptions as complex fluids with network-like structures. Continued development of new dye functionalities [65,66], imaging hardware [67], and analytical tools [68] will help with uncovering spatiotemporal organization and dynamics within condensates, thus enabling direct assessments of structure-function relationships of biomolecular condensates.

Acknowledgments

We are grateful to J. Lu, N.A. Erkamp, and M-K. Shinn for help with the experiments. We thank T. Mittag and W.B. Borcherds for sharing their protocol for the expression and purification of the A1-LCD protein, and we thank L.E. Kay for sharing the DDX4 gene. This work was funded by the Air Force Office of Scientific Research grant (to RVP), the St. Jude Research Collaborative on the Biology and Biophysics of RNP granules (to RVP), and the National Institutes of Health (F32GM146418-01A1 to MRK and R35GM124858 to MDL). RVP and MDL are members of the Center for Biomolecular Condensates in the James McKelvey School of Engineering at Washington University in St. Louis.

Author contributions

RVP and MDL conceived of and supervised the research. TW designed and performed the imaging experiments and analyzed the data with inputs from MDL and RVP. MRK prepared A1-LCD, Aro^{+}, Aro^{-}, and DDX4 proteins, performed phase separation assays, and contributed intellectual insights. MF performed the LaSSI simulations and analyzed the simulation results. TW, MDL, and RVP wrote and edited the manuscript with input from all authors.

Competing interests

RVP is a member of the scientific advisory board of and shareholder at Dewpoint Therapeutics Inc. The work reported here was not influenced by this affiliation. The remaining authors have no competing interests to declare.

Additional information

Details of the imaging methods, analysis of images, constructs used, the preparation of condensates, LaSSI simulations, additional data and supplemental figures are presented in the supplementary material. Correspondence and requests for materials should be addressed to RVP and MDL.

References

1 Banani, S. F., Lee, H. O., Hyman, A. A. & Rosen, M. K. Biomolecular condensates: organizers of cellular biochemistry. *Nature reviews. Molecular cell biology* **18**, 285-298, doi:10.1038/nrm.2017.7 (2017).

2 Bremer, A. *et al.* Deciphering how naturally occurring sequence features impact the phase behaviours of disordered prion-like domains. *Nature Chemistry* **14**, 196-207, doi:10.1038/s41557-021-00840-w (2022).

3 Nott, Timothy J. *et al.* Phase Transition of a Disordered Nuage Protein Generates Environmentally Responsive Membraneless Organelles. *Molecular Cell* **57**, 936-947, doi:https://doi.org/10.1016/j.molcel.2015.01.013 (2015).

4 Jawerth, L. *et al.* Protein condensates as aging Maxwell fluids. *Science* **370**, 1317-1323, doi:10.1126/science.aaw4951 (2020).

5 Ghosh, A., Kota, D. & Zhou, H.-X. Shear relaxation governs fusion dynamics of biomolecular condensates. *Nature Communications* **12**, 5995, doi:10.1038/s41467-021-26274-z (2021).

6 Alshareedah, I., Moosa, M. M., Pham, M., Potoyan, D. A. & Banerjee, P. R. Programmable Viscoelasticity in Protein-RNA Condensates with Disordered Sticker-Spacer Polypeptides. *Nature Communications* **12**, 6620, doi:10.1101/2021.01.24.427968 (2021).

7 Feric, M. *et al.* Coexisting Liquid Phases Underlie Nucleolar Subcompartments. *Cell* **165**, 1686-1697, doi:10.1016/j.cell.2016.04.047 (2016).

8 Bergeron-Sandoval, L. P. *et al.* Endocytic proteins with prion-like domains form viscoelastic condensates that enable membrane remodeling. *Proceedings of the National Academy of Sciences* **118**, e2113789118, doi:10.1073/pnas.2113789118 (2021).

9 Alshareedah, I. *et al.* Sequence-encoded grammars determine material properties and physical aging of protein condensates. *bioRxiv*, 2023.2004.2006.535902, doi:10.1101/2023.04.06.535902 (2023).

10 Wróbel, J. K., Cortez, R. & Fauci, L. Modeling viscoelastic networks in Stokes flow. *Physics of Fluids* **26**, 113102, doi:10.1063/1.4900941 (2014).

11 Michieletto, D. & Marenda, M. Rheology and Viscoelasticity of Proteins and Nucleic Acids Condensates. *JACS Au* **2**, 1506-1521, doi:10.1021/jacsau.2c00055 (2022).

12 Farag, M. *et al.* Condensates formed by prion-like low-complexity domains have small-world network structures and interfaces defined by expanded conformations. *Nature Communications* **13**, 7722, doi:10.1038/s41467-022-35370-7 (2022).

13 Farag, M., Borcherds, W. M., Bremer, A., Mittag, T. & Pappu, R. V. Phase separation of protein mixtures is driven by the interplay of homotypic and heterotypic interactions. *Nature Communications* **14**, 5527, doi:10.1038/s41467-023-41274-x (2023).

14 Taylor, N. *et al.* Biophysical characterization of organelle-based RNA/protein liquid phases using microfluidics. *Soft Matter* **12**, 9142-9150, doi:10.1039/C6SM01087C (2016).

15 Hyman, A. A., Weber, C. A. & Jülicher, F. Liquid-liquid phase separation in biology. *Annu. Rev. Cell Dev. Biol.* **30**, 39-58, doi:10.1146/annurev-cellbio-100913-013325 (2014).

16 Grimm, J. B., Heckman, L. M. & Lavis, L. D. in *Progress in Molecular Biology and Translational Science* Vol. 113 (ed May C. Morris) 1-34 (Academic Press, 2013).

17 Martinez, V. & Henary, M. Nile Red and Nile Blue: Applications and Syntheses of Structural Analogues. *Chemistry – A European Journal* **22**, 13764-13782, doi:https://doi.org/10.1002/chem.201601570 (2016).

18 Verkman, A. S. Mechanism and kinetics of merocyanine 540 binding to phospholipid membranes. *Biochemistry* **26**, 4050-4056, doi:10.1021/bi00387a046 (1987).

19 Li, H. & Vaughan, J. C. Switchable Fluorophores for Single-Molecule Localization Microscopy. *Chemical Reviews* **118**, 9412-9454, doi:10.1021/acs.chemrev.7b00767 (2018).

20 Lew, M. D. *et al.* Three-dimensional superresolution colocalization of intracellular protein superstructures and the cell surface in live Caulobacter crescentus. *Proceedings of the National Academy of Sciences* **108**, E1102-E1110, doi:doi:10.1073/pnas.1114444108 (2011).

21 Spehar, K. *et al.* Super-resolution Imaging of Amyloid Structures over Extended Times by Using Transient Binding of Single Thioflavin T Molecules. *ChemBioChem* **19**, 1944-1948, doi:https://doi.org/10.1002/cbic.201800352 (2018).

22 Danylchuk, D. I., Moon, S., Xu, K. & Klymchenko, A. S. Switchable Solvatochromic Probes for Live-Cell Super-resolution Imaging of Plasma Membrane Organization. *Angewandte Chemie International Edition* **58**, 14920-14924, doi:https://doi.org/10.1002/anie.201907690 (2019).

23 Ding, T., Wu, T., Mazidi, H., Zhang, O. & Lew, M. D. Single-molecule orientation localization microscopy for resolving structural heterogeneities between amyloid fibrils. *Optica* **7**, 602-607, doi:10.1364/OPTICA.388157 (2020).

24 Lu, J., Mazidi, H., Ding, T., Zhang, O. & Lew, M. D. Single-Molecule 3D Orientation Imaging Reveals Nanoscale Compositional Heterogeneity in Lipid Membranes. *Angewandte Chemie International Edition* **59**, 17572-17579, doi:https://doi.org/10.1002/anie.202006207 (2020).

25 Hou, Y., Bardo, A. M., Martinez, C. & Higgins, D. A. Characterization of Molecular Scale Environments in Polymer Films by Single Molecule Spectroscopy. *The Journal of Physical Chemistry B* **104**, 212-219, doi:10.1021/jp992312y (2000).

26 Sackett, D. L., Knutson, J. R. & Wolff, J. Hydrophobic surfaces of tubulin probed by time-resolved and steady-state fluorescence of nile red. *Journal of Biological Chemistry* **265**, 14899-14906, doi:https://doi.org/10.1016/S0021-9258(18)77201-3 (1990).

27 Tajalli, H., Gilani, A. G., Zakerhamidi, M. S. & Tajalli, P. The photophysical properties of Nile red and Nile blue in ordered anisotropic media. *Dyes and Pigments* **78**, 15-24, doi:https://doi.org/10.1016/j.dyepig.2007.10.002 (2008).

28 Martin, E. W. *et al.* Valence and patterning of aromatic residues determine the phase behavior of prion-like domains. *Science* **367**, 694-699, doi:10.1126/science.aaw8653 (2020).

29 Brady, J. P. *et al.* Structural and hydrodynamic properties of an intrinsically disordered region of a germ cell-specific protein on phase separation. *Proceedings of the National Academy of Sciences USA* **114**, E8194-E8203, doi:doi:10.1073/pnas.1706197114 (2017).

30 Alshareedah, I., Kaur, T. & Banerjee, P. R. Methods for characterizing the material properties of biomolecular condensates. *Methods in Enzymology* **646**, 143-183, doi:10.1016/bs.mie.2020.06.009 (2021).

31 Kaur, T. *et al.* Sequence-encoded and composition-dependent protein-RNA interactions control multiphasic condensate morphologies. *Nature Communications* **12**, 872, doi:10.1038/s41467-021-21089-4 (2021).

32 Shillcock, J. C., Lagisquet, C., Alexandre, J., Vuillon, L. & Ipsen, J. H. Model biomolecular condensates have heterogeneous structure quantitatively dependent on the interaction profile of their constituent macromolecules. *Soft Matter*, 10.1039/D1032SM00387B, doi:10.1039/D2SM00387B (2022).

33 Böddeker, T. J. *et al.* Non-specific adhesive forces between filaments and membraneless organelles. *Nature Physics* **18**, 571-578, doi:10.1038/s41567-022-01537-8 (2022).

34 Feric, M. *et al.* Mesoscale structure–function relationships in mitochondrial transcriptional condensates. *Proceedings of the National Academy of Sciences* **119**, e2207303119, doi:doi:10.1073/pnas.2207303119 (2022).

35 Sharonov, A. & Hochstrasser, R. M. Wide-field subdiffraction imaging by accumulated binding of diffusing probes. *Proceedings of the National Academy of Sciences* **103**, 18911-18916, doi:doi:10.1073/pnas.0609643104 (2006).

36 Ruff, K. M., Dar, F. & Pappu, R. V. Ligand effects on phase separation of multivalent macromolecules. *Proceedings of the National Academy of Sciences USA* **118**, e2017184118, doi:10.1073/pnas.2017184118 (2021).

37 Ruff, K. M., Dar, F. & Pappu, R. V. Polyphasic linkage and the impact of ligand binding on the regulation of biomolecular condensates. *Biophysics Reviews* **2**, 021302, doi:10.1063/5.0050059 (2021).

38 Kulinich, A. V. & Aleksandr, A. I. Merocyanine dyes: synthesis, structure, properties and applications. *Russian Chemical Reviews* **78**, 141, doi:10.1070/RC2009v078n02ABEH003900 (2009).

39 Greenspan, P. & Fowler, S. D. Spectrofluorometric studies of the lipid probe, nile red. *Journal of Lipid Research* **26**, 781-789, doi:https://doi.org/10.1016/S0022-2275(20)34307-8 (1985).

40 Kuo, C. & Hochstrasser, R. M. Super-resolution Microscopy of Lipid Bilayer Phases. *Journal of the American Chemical Society* **133**, 4664-4667, doi:10.1021/ja1099193 (2011).

41 Lelek, M. *et al.* Single-molecule localization microscopy. *Nature Reviews Methods Primers* **1**, 39, doi:10.1038/s43586-021-00038-x (2021).

42 Betzig, E. *et al.* Imaging Intracellular Fluorescent Proteins at Nanometer Resolution. *Science* **313**, 1642-1645, doi:doi:10.1126/science.1127344 (2006).

43 Hess, S. T., Girirajan, T. P. K. & Mason, M. D. Ultra-High Resolution Imaging by Fluorescence Photoactivation Localization Microscopy. *Biophysical Journal* **91**, 4258-4272, doi:https://doi.org/10.1529/biophysj.106.091116 (2006).

44 Rust, M. J., Bates, M. & Zhuang, X. Sub-diffraction-limit imaging by stochastic optical reconstruction microscopy (STORM). *Nature Methods* **3**, 793-796, doi:10.1038/nmeth929 (2006).

45 Chhabra, R. Nonwoven Uniformity — Measurements Using Image Analysis. *International Nonwovens Journal* **os-12**, 1558925003os-1551200112, doi:10.1177/1558925003os-1200112 (2003).

46 Ripley, B. D. Modelling Spatial Patterns. *Journal of the Royal Statistical Society: Series B (Methodological)* **39**, 172-192, doi:https://doi.org/10.1111/j.2517-6161.1977.tb01615.x (1977).

47 Khater, I. M., Nabi, I. R. & Hamarneh, G. A Review of Super-Resolution Single-Molecule Localization Microscopy Cluster Analysis and Quantification Methods. *Patterns* **1**, doi:10.1016/j.patter.2020.100038 (2020).

48 Malkusch, S. *et al.* Coordinate-based colocalization analysis of single-molecule localization microscopy data. *Histochemistry and Cell Biology* **137**, 1-10, doi:10.1007/s00418-011-0880-5 (2012).

49 Shen, M. *et al.* Nanoscale Colocalization of Fluorogenic Probes Reveals the Role of Oxygen Vacancies in the Photocatalytic Activity of Tungsten Oxide Nanowires. *ACS Catalysis* **10**, 2088-2099, doi:10.1021/acscatal.9b04481 (2020).

50 Pappu, R. V., Cohen, S. R., Dar, F., Farag, M. & Kar, M. Phase Transitions of Associative Biomacromolecules. *Chemical Reviews* **123**, 8945-8987, doi:10.1021/acs.chemrev.2c00814 (2023).

51 Stillwell, W. *et al.* Use of merocyanine (MC540) in quantifying lipid domains and packing in phospholipid vesicles and tumor cells. *Biochimica et Biophysica Acta (BBA) - Biomembranes* **1146**, 136-144, doi:https://doi.org/10.1016/0005-2736(93)90348-4 (1993).

52 Wu, T., Lu, J. & Lew, M. D. Dipole-spread-function engineering for simultaneously measuring the 3D orientations and 3D positions of fluorescent molecules. *Optica* **9**, 505-511, doi:10.1364/OPTICA.451899 (2022).

53 Erkamp, N. A. *et al.* Adsorption of RNA to interfaces of biomolecular condensates enables wetting transitions. *bioRxiv*, 2023.2001.2012.523837, doi:10.1101/2023.01.12.523837 (2023).

54 He, C., Wu, C. Y., Li, W. & Xu, K. Multidimensional Super-Resolution Microscopy Unveils Nanoscale Surface Aggregates in the Aging of FUS Condensates. *Journal of the American Chemical Society*, doi:10.1021/jacs.3c08674 (2023).

55 Thody, S. A. *et al.* Small Molecule Properties Define Partitioning into Biomolecular Condensates. *bioRxiv*, 2022.2012.2019.521099, doi:10.1101/2022.12.19.521099 (2022).

56 Vernon, R. M. *et al.* Pi-Pi contacts are an overlooked protein feature relevant to phase separation. *eLife* **7**, e31486, doi:10.7554/eLife.31486 (2018).

57 Hong, Y. *et al.* Hydrophobicity of arginine leads to reentrant liquid-liquid phase separation behaviors of arginine-rich proteins. *Nature Communications* **13**, 7326, doi:10.1038/s41467-022-35001-1 (2022).

58 Fossat, M. J., Zeng, X. & Pappu, R. V. Uncovering Differences in Hydration Free Energies and Structures for Model Compound Mimics of Charged Side Chains of Amino

Acids. *The Journal of Physical Chemistry B* **125**, 4148-4161, doi:10.1021/acs.jpcb.1c01073 (2021).

59 Jain, S. *et al.* ATPase-Modulated Stress Granules Contain a Diverse Proteome and Substructure. *Cell* **164**, 487-498, doi:https://doi.org/10.1016/j.cell.2015.12.038 (2016).

60 Pederson, T. The Nucleolus. *Cold Spring Harbor Perspectives in Biology* **3**, doi:10.1101/cshperspect.a000638 (2011).

61 Fei, J. *et al.* Quantitative analysis of multilayer organization of proteins and RNA in nuclear speckles at super resolution. *Journal of Cell Science* **130**, 4180-4192 (2017).

62 Simon, J. R., Carroll, N. J., Rubinstein, M., Chilkoti, A. & López, G. P. Programming molecular self-assembly of intrinsically disordered proteins containing sequences of low complexity. *Nature Chemistry* **9**, 509-515, doi:10.1038/nchem.2715 (2017).

63 Harmon, T. S., Holehouse, A. S. & Pappu, R. V. Differential solvation of intrinsically disordered linkers drives the formation of spatially organized droplets in ternary systems of linear multivalent proteins. *New Journal of Physics* **20**, 045002, doi:10.1088/1367-2630/aab8d9 (2018).

64 Handwerger, K. E., Cordero, J. A. & Gall, J. G. Cajal Bodies, Nucleoli, and Speckles in the Xenopus Oocyte Nucleus Have a Low-Density, Sponge-like Structure. *Molecular Biology of the Cell* **16**, 202-211, doi:10.1091/mbc.e04-08-0742 (2005).

65 Needham, L.-M. *et al.* ThX – a next-generation probe for the early detection of amyloid aggregates. *Chemical Science* **11**, 4578-4583, doi:10.1039/C9SC04730A (2020).

66 Aparin, I. O. *et al.* Fluorogenic Dimers as Bright Switchable Probes for Enhanced Super-Resolution Imaging of Cell Membranes. *Journal of the American Chemical Society* **144**, 18043-18053, doi:10.1021/jacs.2c07542 (2022).

67 Zhang, O. *et al.* Six-dimensional single-molecule imaging with isotropic resolution using a multi-view reflector microscope. *Nature Photonics* **17**, 179-186, doi:10.1038/s41566-022-01116-6 (2023).

68 Schröder, T. *et al.* Shrinking gate fluorescence correlation spectroscopy yields equilibrium constants and separates photophysics from structural dynamics. *Proceedings of the National Academy of Sciences* **120**, e2211896120, doi:doi:10.1073/pnas.2211896120 (2023).